applied sciences

MDPI

Article

Duty Factor Reflects Lower Limb Kinematics of Running

Aurélien Patoz [1,2,*], Thibault Lussiana [3,4], Adrien Thouvenot [3,4], Laurent Mourot [4,5] and Cyrille Gindre [2]

1 Institute of Sport Sciences, University of Lausanne, 1015 Lausanne, Switzerland
2 Research and Development Department, Volodalen Swiss Sport Lab, 1860 Aigle, Switzerland; cyrille@volodalen.com
3 Research and Development Department, Volodalen, 39270 Chavéria, France; thibault@volodalen.com (T.L.); adrien@volodalen.com (A.T.)
4 Research Unit EA3920 Prognostic Markers and Regulatory Factors of Cardiovascular Diseases and Exercise Performance, Health, Innovation Platform, University of Bourgogne Franche-Comté, 25000 Besançon, France; laurent.mourot@univ-fcomte.fr
5 Division for Physical Education, Tomsk Polytechnic University, 634040 Tomsk, Russia
* Correspondence: aurelien.patoz@unil.ch; Tel.: +41-79-535-07-16

Received: 27 October 2020; Accepted: 5 December 2020; Published: 9 December 2020

Abstract: The aim was to identify the differences in lower limb kinematics used by high (DF_{high}) and low (DF_{low}) duty factor (DF) runners, particularly their sagittal plane (hip, knee, and ankle) joint angles and pelvis and foot segment angles during stance. Fifty-nine runners were divided in two DF groups based on their mean DF measured across a range of speeds. Temporal characteristics and whole-body three-dimensional kinematics of the running step were recorded from treadmill runs at 8, 10, 12, 14, 16, and 18 km/h. Across speeds, DF_{high} runners, which limit vertical displacement of the COM and promote forward propulsion, exhibited more lower limb flexion than DF_{low} during the ground contact time and were rearfoot strikers. On the contrary, DF_{low} runners used a more extended lower limb than DF_{high} due to a stiffer leg and were midfoot and forefoot strikers. Therefore, two different lower limb kinematic mechanisms are involved in running and the one of an individual is reflected by the DF.

Keywords: biomechanics; running pattern; self-optimization

1. Introduction

In both well-trained athletes and recreational runners, a U-shaped curvilinear relationship between running economy and self-selected stride length [1–7], stride rate [3,7], and contact time (t_c) or leg stiffness [8] has been reported. This highlights that runners seem to self-optimize their running gait to minimize the metabolic cost of running [1,9–11].

An emergent area of research is focusing on the individual runner to try to identify how the person's structure and functional abilities influence performance, running economy, or running-related injuries [12]. For instance, self-organizing map [13] or hierarchical cluster analysis [14] approaches identified different running gait strategies within a given sample of runner. Based on a subjective evaluation of the spontaneous overall running pattern, other researchers categorized runners in two groups with kinematic differences, called terrestrial and aerial runners [15,16]. Using the duty factor (DF; an objective parameter representing the proportion of time spent in contact with the ground during a running stride), Lussiana et al. (2019) observed global biomechanical differences when classifying runners in two groups called DF_{low} (a low mean DF ($\overline{DF}$) averaged over different running speeds) and

DF_{high} (a high $\overline{DF}$) [17]. In their analysis, the authors divided the running cycle in several subtimings, namely, braking (t_b) and pushing (t_p) times, which are defined from footstrike (FS) to mid-stance (MS) and from MS to toe-off (TO), respectively, and elevation (t_e) and dropping (t_d) times, defined as the time from TO to mid-flight (MF) and from MF to FS of the contralateral foot, respectively. MS and MF events were calculated to divide t_c and flight time (t_f), respectively. The authors observed that the two subcomponents of the contact phase (t_b and t_p) were statistically longer for DF_{high} than for DF_{low} and that both t_e and t_d were statistically shorter for DF_{high} than for DF_{low}. In addition, the authors showed that the vertical displacement of the center of mass (COM) during the elevation phase ($\Delta z_{COM,e}$) was statistically greater for DF_{low} than for DF_{high}, but no statistical differences were obtained for the vertical displacement of the COM during braking ($\Delta z_{COM,b}$), pushing ($\Delta z_{COM,p}$), and dropping ($\Delta z_{COM,d}$) phases.

Similar subgroupings of participants were obtained based on the DF measured at 12 km/h than based on a subjective evaluation of the spontaneous overall running pattern [18]. The two groups of runners have the same running economy, but with a different running pattern: aerial and DF_{low} favor a long t_f together with a midfoot to forefoot strike pattern. On the contrary, terrestrial and DF_{high} favor a long t_c associated with a rearfoot strike pattern [17,19]. Moreover, grouping runners based on their DF reflect their global running pattern, which takes into account not only the FS pattern but also vertical oscillation of the head, antero-posterior motion of the elbows, vertical pelvis position at ground contact, and antero-posterior foot position at ground contact. Similarly to what was observed when grouping runners based on their global running pattern, no difference in running economy has been reported while using more local and finer parameters, such as the FS angle [20] or strike pattern [21–23].

Beyond metabolic cost, different FS patterns are providing different impact loading rates. Using a forefoot strike pattern does not eliminate the passive impact peak at the ground contact [22]. This passive impact peak usually occurs at about 25 ms after initial ground contact and this event marks the middle of the passive peak impact attenuation (IA) phase [24–32]. Both passive and active impact peaks need to be attenuated and different strategies for impact attenuation have been observed [33,34]. Forefoot strikers were shown to have a greater reliance on soft tissues (active mechanisms) [34,35] whereas rearfoot runners were shown to more prominently attenuate the impact using passive mechanisms [24,34], but also using active mechanisms [36,37]. Indeed, the heel pad of the foot and skeletal tissue are absorbing most of the shock when rearfoot striking [24,34]. In addition, the eccentric action of the knee extensor [37] and dorsiflexor [36] muscles during t_c were also shown to play a role. As for running with a forefoot strike pattern, the eccentric action of the plantar flexor muscles during t_c, acting as a shock absorber, is required [25,38,39]. These impact attenuation strategies between forefoot and rearfoot strike patterns induce different loadings on the lower limb and different three-dimensional (3D) stress patterns in the ankle, knee, and hip joint [40–42], and different sagittal plane (hip, knee, and ankle) joint angles and pelvis and foot segment angles during stance [42,43], but with no global advantage of one strike pattern over the other [40].

Following verbal instructions directing the runners towards a more compliant running stride, rearfoot strikers were able to adopt a higher degree of knee and hip flexions during t_c [44]. Similarly, "Groucho" running [45] shows global body flexion while "Pose" running [46] uses an extended posture albeit the greater knee flexion at initial contact. Therefore, these observations suggest the existence of global running patterns associated with specific lower limb kinematics.

Hence, the classification of runners based on their $\overline{DF}$ showed the existence of two different self-optimized global running patterns [17]. However, nothing is known about their lower limb kinematics, particularly their sagittal plane (hip, knee, and ankle) joint angles and pelvis and foot segment angles during stance. Therefore, the purpose of this study was to identify the lower limb kinematics for both DF_{high} and DF_{low}. As DF_{high} and DF_{low} favor long t_c and long t_f (therefore shorter relative t_c), respectively, we hypothesized that these two DF groups would rely on two different lower limb kinematic mechanisms. More specifically, we hypothesized that DF_{high} would use more lower limb flexion during t_c than DF_{low}.

2. Materials and Methods

2.1. Participants

The study was conducted during two months between September and October 2017, which permitted to test 59 participants, out of which 42 were males (age: 36.9 ± 9.5 y, height: 1.77 ± 0.06 m, leg length: 0.84 ± 0.04 m, body mass: 72.1 ± 10.0 kg, running time: 4.6 ± 2.3 h/week, and running distance: 43.8 ± 23.2 km/week) and 17 were females (age: 36.1 ± 8.2 y, height: 1.65 ± 0.07 m, leg length: 0.79 ± 0.05 m, body mass: 58.7 ± 6.9 kg, running time: 3.8 ± 1.9 h/week, and running distance: 34.9 ± 16.5 km/week). All participants had been running regularly for at least two years at the time of their study participation. Inclusion criteria were good self-reported general health and no current or recent (<3 months) lower-extremity injury. The university's institutional review board approved the study protocol prior to participant recruitment (CPP: 2014-A00336-41), which was conducted in accordance with international ethical standards, and adhered to the last Declaration of Helsinki of the World Medical Association.

2.2. Experimental Procedure

Each participant completed one experimental session in the laboratory. Running bouts were always performed under similar environmental conditions (23 ± 2 °C and 45 ± 7% relative humidity). All participants were advised to avoid strenuous exercise the day before the test. After providing written informed consent, retroreflective markers were positioned on participants (described in Subsec. Data Collection) to assess their running biomechanics. As for each participant, first, a 5-s standing static trial using a standard anatomical position was recorded on a treadmill (Medic 2850, TMS, Champs sur Yonne, France) for calibration purposes. Then, a 10-min warm-up run was performed on the same treadmill. The running speed could be freely chosen and modified during the 10-min run by the participant. This was followed, after a 1-min break, by six 30-s runs at 8, 10, 12, 14, 16, and 18 km/h (with 1-min recovery periods on the treadmill between each run). 3D kinematic data were collected during the static trial and the last 15 s (22 ± 2 running strides) of the running trials. All participants were familiar with running on a treadmill as part of their usual training program and wore their habitual running shoes during testing.

2.3. Running Gait Classification

The 59 participants were ranked according to their $\overline{DF}$, i.e., the average over six runs performed at 8, 10, 12, 14, 16, and 18 km/h, and classified in two groups. The number of participants being odd, one group had an extra runner. The runner with the 30th $\overline{DF}$ corresponded to the median runner and has been attributed to the DF_{high} group, but attributing him to the DF_{low} group or removing him from the study would not have had an impact on the results. Runners with the 30 highest $\overline{DF}$ were attributed to the DF_{high} group. The DF_{low} group was composed of the runners with the 29 lowest $\overline{DF}$. As Lussiana et al. (2019) observed a significantly larger DF for DF_{high} than DF_{low} at all speeds examined, $\overline{DF}$ is a reliable parameter to rank participants.

2.4. Data Collection

Whole-body 3D kinematic data were collected at 179 Hz using eight infrared Oqus 500+ cameras and the Qualisys Track Manager software version 2018.1, build 4100 (Qualisys AB, Göteborg, Sweden). The laboratory coordinate system was oriented such that the *x*-, *y*-, and *z*-axis denoted the medio-lateral (pointing towards the right side of the body), postero-anterior, and infero-superior axis, respectively. Forty-five and 41 retro-reflective markers of 12 mm diameter were used for static and running trials, respectively. They were affixed to the skin and shoes of individuals over anatomical landmarks using double-sided tape following standard guidelines from the Project Automation Framework Running package [47], and as already reported in Lussiana et al. (2019).

The 3D marker data were exported in .c3d format and processed in Visual3D Professional software version 6.01.12 (C-Motion Inc., Germantown, MD, USA). More explicitly, the 3D marker data were interpolated using a third-order polynomial least-square fit algorithm (using three frames of data before and after the "gap" to calculate the coefficients of the polynomial), allowing a maximum of 20 frames for gap filling, and subsequently low-pass filtered at 20 Hz using a fourth-order Butterworth filter.

2.5. Biomechanical Parameters

From the marker set, a full-body biomechanical model with six degrees of freedom and 15 rigid segments was constructed. Segments included the head, upper arms, lower arms, hands, thorax, pelvis, thighs, shanks, and feet. In Visual3D software, segments were treated as geometric objects. Segments were assigned inertial properties and center of mass locations based on their shape [48] and attributed relative mass based on standard regression equations [49]. Kinematic parameters were calculated using rigid-body analysis and whole-body COM location was calculated from the parameters of all 15 segments (COM was directly provided by Visual3D). Lower limb joint angles (hip, knee, and ankle) were defined as the orientation of the distal segment relative to the proximal one [50] and computed using an *x*–*y*–*z* Cardan sequence [51,52]. For example, the knee joint angle was computed as the orientation of the shank relative to the thigh. Using the proximal segment as the reference segment makes the *x*–*y*–*z* Cardan sequence equivalent to the joint coordinate system [52,53], leading to rotations with functional and anatomical meaning (flexion–extension, abduction–adduction, and internal–external rotation). Segment angles (pelvis and foot) were defined as the orientation of a specific segment relative to the laboratory coordinate system and were also computed using an *x*–*y*–*z* Cardan sequence. These segment angles have also functional meaning that are retroversion-anteversion, negative drop-positive drop, and external–internal rotation for the pelvis and forefoot-rearfoot angle, pronation–supination, and toe-out–toe-in for the foot.

Running events were derived from the kinematic data. More explicitly, mid-toe and mid-foot landmarks were created midway between the first and fifth toe markers, and the heel marker and mid-toe landmark, respectively. The mid-toe landmark was rescaled by subtracting its respective global minimum. Moreover, heel and mid-toe accelerations were calculated as the second derivative of the heel marker and mid-toe landmark, respectively. As for each running trial, FS was defined as the first acceleration spike between the heel marker and mid-toe landmark acceleration spikes. TO was defined as the instance when the mid-toe reached 1 cm on ascent.

t_c and swing time (t_s) were defined as the time from FS to TO and from TO to FS of the same foot, respectively, and t_f as the time from TO of a given foot to FS of the contralateral foot. MS was defined as the instant when the COM reached its lowest vertical position during t_c while MF was defined as the instant when the COM reached its highest vertical position during t_f. The end of the IA phase was set at 50 ms after FS for every runner due to several reasons: (1) the passive impact peak of forefoot strikers is not identifiable without a force platform, (2) runners showing a passive impact peak have a large variability in the timing of this peak around 25 ms, and (3) this peak was shown to occur around 25 ms for speeds ranging from 3 to 5.5 m/s [28]. Passive peak attenuation time (t_a) was defined as the time from FS to IA, i.e., 50 ms. All events were verified to ensure correct identification and were manually adjusted when required. Values for t_c, t_a, t_b, t_p, t_f, t_e, t_d, and t_s were calculated based on FS, IA, MS, TO, and MF events, and DF was calculated as follows [54]

$$\mathrm{DF} = \frac{t_c}{t_c + t_s} \tag{1}$$

All COM positions and displacements were expressed as a percentage of participant's height. Temporal characteristics and COM positions and displacements were given as the average between right and left values.

The joint and segment angles (θ) were calculated at FS, IA, MS, and TO together with their range of motions during the attenuation phase ($\Delta\theta_a$; from FS to IA), braking phase ($\Delta\theta_b$; from FS to MS),

and pushing phase ($\Delta\theta_p$; from MS to TO). Joint and segment angles were given as the average between right and left joint and segment angles, respectively. Segment angles were expressed as a difference with respect to segment angles in the static upright stance.

As for joint angles, we only kept the first Cardan angle, i.e., the rotation about the laterally directed x-axis (flexion–extension) because of possible errors due to kinematic crosstalk [55–57]. As for segment angles, the three Cardan angles were considered. Nonetheless, segment angles in the frontal and transversal planes were presented in Supplementary Materials, as they do not represent flexion–extension of the lower limb. The x-axis being directed laterally for the right-side segments and medially for the left-side segments, the left limb segment angles corresponding to a rotation about the antero-posterior y-axis and infero-superior z-axis were multiplied by –1 in order to maintain the same anatomical polarity between right and left segment angles and to ensure a correct averaging process.

The "running wheel", defined as the vertical position versus antero-posterior position of the COM of the foot segment (the motion of the foot COM in the sagittal plane), was calculated during the running stride. These positions were expressed as a percentage of participant's leg length. The leg length was defined as the average between right and left magnitudes of the 3D vector going from the hip joint to the ankle joint and calculated from the standing static trial.

2.6. Statistical Analysis

Assuming a medium effect size of 0.5 [58], an α error of 0.05, and a power of 0.8, standard sample size calculations have led to the requirement of 54 participants, however the 59 participants were kept to slightly increase statistical power [59]. Descriptive statistics are presented using mean ± standard deviation. After inspecting residual plots, no obvious deviations from homoscedasticity, homogeneity of variances, or normality were present. Unpaired two-sided Student's t-tests were used to compare participant characteristics between DF groups. Two-way (DF groups × running speed) repeated measures ANOVA with Mauchly's correction for sphericity and employing Holm procedures for pair-wise post-hoc comparisons were used to investigate whether biomechanical parameters differed between DF_{high} and DF_{low} groups, while accounting for the effect of running speed. Cohen's d effect size was calculated when a significant DF groups main effect was observed [58], and classified as small, moderate, and large when d values were larger than 0.2, 0.5, and 0.8, respectively [58]. Statistical analysis was performed using Jamovi (version 1.0.8, (Computer Software), Retrieved from https://www.jamovi.org) and R 3.5.0 (The R Foundation for Statistical Computing, Vienna, Austria) with a level of significance set at $p \leq 0.05$.

3. Results

3.1. Participant Characteristics between DF_{high} and DF_{low} Groups

The baseline characteristics of DF_{high} and DF_{low} together with pelvis and foot segment angles in the static upright stance are given in Table 1 and were similar between groups. The increase of the running speed from 8 to 18 km/h was accompanied with a decrease of the DF from 35.5 ± 2.4% to 26.6 ± 1.5% for DF_{high} while DF_{low} decreased their DF from 29.9 ± 2.2% to 23.1 ± 2.4%.

Table 1. Participant characteristics for the high (DF_{high}) and low (DF_{low}) duty factor running groups.

Characteristics	DF_{high}	DF_{low}	p
sex	M = 21; F = 9	M = 21; F = 8	NA
age (y)	38.7 ± 7.7	34.6 ± 10.0	0.085
height (m)	1.73 ± 0.10	1.74 ± 0.07	0.847
leg length (m)	0.82 ± 0.05	0.83 ± 0.05	0.551
mass (kg)	69.4 ± 13.4	67.1 ± 8.1	0.440
running time (h/week)	4.2 ± 2.2	4.5 ± 2.2	0.515
running distance (km/week)	39.9 ± 20.9	42.6 ± 22.7	0.645
pelvis retroversion–anteversion (deg)	12.3 ± 5.5	10.3 ± 5.5	0.157
pelvis negative–positive drop (deg)	0.1 ± 2.3	−0.2 ± 2.2	0.528
pelvis external–internal rotation (deg)	0.4 ± 2.4	−0.1 ± 2.4	0.482
forefoot–rearfoot (deg)	−21.1 ± 3.2	−22.1± 3.0	0.225
foot pronation–supination (deg)	16.4 ± 3.2	17.2 ± 3.0	0.281
toe-out–toe-in (deg)	−15.8 ± 5.0	−14.7 ± 5.2	0.386
$\overline{DF}$ (%)	30.6 ± 2.2	26.0 ± 2.5	NA

Note: data are means ± standard deviation. $\overline{DF}$: average of the duty factors obtained from the data collected at several running speeds, M: male, F: female, and NA: not applicable.

3.2. Temporal Characteristics and Center of Mass Displacement

The two subcomponents of the contact phase (t_b and t_p) were longer for DF_{high} than for DF_{low} (DF groups main effect, $p < 0.001$; t_b: moderate effect size, $d = 0.62$ and t_p: large effect size, $d = 0.82$; Table 2 and Figure 1). The opposite was observed for t_e and t_d (DF groups main effect, $p < 0.001$; large effect size, $d \geq 1.37$; Table 2 and Figure 1), with greater values for DF_{low} than for DF_{high}. Running speed affected all temporal parameters, with a decrease of t_b and t_p and an increase of t_e and t_d with increasing running speed (speed main effect, $p < 0.001$; Table 2). Interaction effects were observed for all temporal parameters, indicating a decrease of t_b and t_p and an increase of t_e and t_d (all $p \leq 0.01$; Table 2) with the increase of running speed for both DF groups.

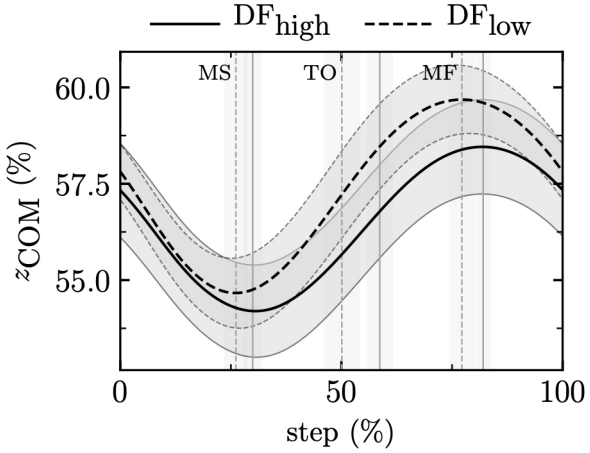

Figure 1. Vertical position of the center of mass (z_{COM}) during the running step for the high (DF_{high}) and low (DF_{low}) duty factor running groups while running at 14 km/h. z_{COM} is expressed as a percentage of participant's height. The running speed represented is representative of all speed. MS: mid-stance, TO: toe-off, and MF: mid-flight.

Table 2. Temporal parameters (t_b, t_p, t_e, and t_d) of the running step and vertical displacements (Δz_b, Δz_p, Δz_e, and Δz_d) of the center of mass (COM) during the running step for the high (DF_{high}) and low (DF_{low}) duty factor running groups at the different running speeds.

–		FS to MS		MS to TO		TO to MF		MF to FS	
Running Speed (km/h)	**DF Group**	t_b **(ms)**	$\Delta z_{COM,b}$ **(%)**	t_p **(ms)**	$\Delta z_{COM,p}$ **(%)**	t_e **(ms)**	$\Delta z_{COM,e}$ **(%)**	t_d **(ms)**	$\Delta z_{COM,d}$ **(%)**
8	DF_{high}	129 ± 14	−3.7 ± 0.5	133 ± 11	3.4 ± 0.4	61 ± 13	1.0 ± 0.4	46 ± 11	−0.7 ± 0.3
	DF_{low}	114 ± 12 *	−4.0 ± 0.6	111 ± 12 *	3.4 ± 0.5	83 ± 11 *	2.0 ± 0.5	68 ± 11 *	−1.4 ± 0.4
10	DF_{high}	119 ± 13	−3.8 ± 0.4	117 ± 8	3.2 ± 0.3	70 ± 12	1.4 ± 0.4	52 ± 9	−0.9 ± 0.3
	DF_{low}	104 ± 11 *	−3.7 ± 0.6	98 ± 10 *	3.1 ± 0.5	89 ± 11 *	2.3 ± 0.6	74 ± 9 *	−1.7 ± 0.4
12	DF_{high}	110 ± 11	−3.5 ± 0.4	105 ± 7	2.9 ± 0.2	74 ± 11	1.6 ± 0.4	56 ± 7	−1.0 ± 0.3
	DF_{low}	97 ± 10 *	−3.5 ± 0.5	90 ± 9 *	2.8 ± 0.4	91 ± 9 *	2.4 ± 0.4	76 ± 11 *	−1.8 ± 0.4
14	DF_{high}	99 ± 10	−3.2 ± 0.5	95 ± 7	2.6 ± 0.3	78 ± 11	1.7 ± 0.4	60 ± 6	−1.1 ± 0.3
	DF_{low}	89 ± 10 *	−3.2 ± 0.5	82 ± 8 *	2.6 ± 0.4	93 ± 9 *	2.5 ± 0.5	78 ± 12 *	−1.9 ± 0.5
16	DF_{high}	90 ± 9	−2.9 ± 0.7	87 ± 7	2.3 ± 0.4	79 ± 10	1.8 ± 0.5	62 ± 7	−1.3 ± 0.2
	DF_{low}	82 ± 9 *	−2.8 ± 0.4	75 ± 8 *	2.3 ± 0.4	92 ± 10 *	2.5 ± 0.5	77 ± 12 *	−1.9 ± 0.5
18	DF_{high}	82 ± 10	−2.6 ± 0.5	79 ± 6	2.1 ± 0.3	80 ± 10	1.8 ± 0.5	62 ± 7	−1.3 ± 0.3
	DF_{low}	75 ± 9	−2.5 ± 0.4	69 ± 8 *	2.0 ± 0.4	92 ± 11 *	2.4 ± 0.6	76 ± 14 *	−1.9 ± 0.6
DF groups effect (p)		**<0.001**	0.893	**<0.001**	0.434	**<0.001**	**<0.001**	**<0.001**	**<0.001**
running speed effect (p)		**<0.001**	**<0.001**	**<0.001**	**<0.001**	**<0.001**	**<0.001**	**<0.001**	**<0.001**
interaction effect (p)		**<0.001**	0.056	**<0.001**	0.375	**0.002**	0.061	**0.01**	0.418

Note: data are means ± standard deviation. Duration and corresponding COM displacement of the braking (t_b, $\Delta z_{COM,b}$), pushing (t_p, $\Delta z_{COM,p}$), elevation (t_e, $\Delta z_{COM,e}$), and dropping (t_d, $\Delta z_{COM,d}$) phases are presented. Duration were kept in absolute scale, i.e., were not normalized, to make a distinction between the statistical analyses and the way our groups were created (based on DF, i.e., t_c normalized to the running cycle). COM displacement is expressed as a percentage of participant's height. Significant differences ($p < 0.05$) identified by the two-way repeated measures ANOVA are indicated in bold. * Significant difference between DF groups at a given speed as determined by Holm post-hoc tests. FS: foot strike, MS: mid-stance, TO: toe-off, and MF: mid-flight.

DF_{high} exhibited smaller $\Delta z_{COM,e}$ and $|\Delta z_{COM,d}|$ than DF_{low} (DF groups main effect, $p < 0.001$; large effect size, $d \geq 1.51$; Table 2 and Figure 1). There was a significant decrease of $|\Delta z_{COM,b}|$ and $\Delta z_{COM,p}$ and a significant increase of $\Delta z_{COM,e}$ and $|\Delta z_{COM,d}|$ while running speed increased for both DF groups (running speed main effect, $p < 0.001$; Table 2).

3.3. Hip, Knee, and Ankle Joint Angles

DF_{high} had a larger hip flexion than DF_{low} at FS, IA, and MS (DF groups main effect, $p \leq 0.002$; large effect size, $d \geq 0.81$; Table 3 and Figure 2A). More hip extension during t_p was observed for DF_{high} as depicted by the larger $|\Delta\theta_p|$ (DF groups main effect, $p < 0.001$; medium effect size, $d = 0.75$; Table 3 and Figure 2A). Running speed affected all hip angle parameters, with an increase of the hip flexion at FS, IA, and MS, a decrease at TO, and more hip extension during all subphases of the stance phase with increasing running speed (larger $|\Delta\theta|$; speed main effect, $p < 0.001$; Table 3). An interaction effect between DF groups and speeds was observed for $\Delta\theta_p$, indicating a more pronounced hip extension during t_p (larger $|\Delta\theta_p|$) with the increase of running speed for both DF groups ($p = 0.012$; Table 3).

The knee flexion was larger at MS for DF_{high} than for DF_{low} (DF groups main effect, $p = 0.019$; medium effect size, $d = 0.59$; Table 4 and Figure 2B). DF_{high} exhibited more flexion of the knee during t_b (larger $\Delta\theta_b$) and more extension during t_p (larger $|\Delta\theta_p|$; DF groups main effect, $p \leq 0.019$; medium effect size, $d \geq 0.53$; Table 4 and Figure 2B). Running speed affected all knee angle parameters, with an increase of the knee flexion at the four running events, more flexion of the knee during t_a and t_b (larger $\Delta\theta_a$ and $\Delta\theta_b$), and more extension during t_p with increasing running speed (larger $|\Delta\theta_p|$, speed main effect, $p \leq 0.001$; Table 4). The interaction effect indicated an increase of the knee flexion at IA, more flexion of the knee during t_a (larger $\Delta\theta_a$), and more extension during t_p (larger $|\Delta\theta_p|$) with the increase of running speed for both DF groups ($p \leq 0.029$; Table 4).

Table 3. Hip extension–flexion joint angle at specific events of the running stance (θ_{FS}, θ_{IA}, θ_{MS}, and θ_{TO}) and their range of motions during the different running stance phases ($\Delta\theta_a$, $\Delta\theta_b$, and $\Delta\theta_p$) for the high (DF_{high}) and low (DF_{low}) duty factor running groups at the different running speeds.

Running Speed (km/h)	DF Group	θ_{FS} (deg)	θ_{IA} (deg)	θ_{MS} (deg)	θ_{TO} (deg)	$\Delta\theta_a$ (deg)	$\Delta\theta_b$ (deg)	$\Delta\theta_p$ (deg)
8	DF_{high}	32.0 ± 5.8	29.4 ± 5.8	23.8 ± 5.9	3.0 ± 5.4	−2.6 ± 1.5	−8.1 ± 3.0	−20.9 ± 2.9
	DF_{low}	26.5 ± 6.6	23.5 ± 6.7	19.2 ± 6.9	1.4 ± 5.6	−3.0 ± 1.7	−7.3 ± 2.5	−17.8 ± 3.1 *
10	DF_{high}	35.1 ± 5.9	32.1 ± 5.9	25.9 ± 5.7	1.8 ± 5.0	−3.1 ± 1.7	−9.3 ± 3.0	−24.0 ± 3.1
	DF_{low}	29.1 ± 6.7	25.7 ± 6.8	20.7 ± 6.9	0.2 ± 5.6	−3.5 ± 1.8	−8.4 ± 2.5	−20.6 ± 3.3 *
12	DF_{high}	37.7 ± 5.8	33.8 ± 5.7	27.2 ± 5.5	0.6 ± 4.7	−3.8 ± 2.0	−10.4 ± 3.0	−26.6 ± 3.1
	DF_{low}	31.1 ± 7.1	27.3 ± 7.2	22.0 ± 7.4	−1.2 ± 5.8	−3.8 ± 2.1	−9.1 ± 2.4	−23.1 ± 3.6 *
14	DF_{high}	39.4 ± 5.9	34.9 ± 5.6	28.4 ± 5.8	−0.7 ± 4.6	−4.6 ± 2.3	−11.0 ± 2.9	−29.1 ± 3.5
	DF_{low}	32.7 ± 7.6	28.2 ± 7.7	22.7 ± 7.6	−2.3 ± 6.2	−4.4 ± 2.2	−10.0 ± 2.5	−25.0 ± 3.8 *
16	DF_{high}	40.6 ± 6.1	35.5 ± 5.5	29.4 ± 5.6	−2.0 ± 4.6	−5.1 ± 2.6	−11.2 ± 3.2	−31.4 ± 3.6
	DF_{low}	33.8 ± 8.0	28.6 ±8.2	23.2 ± 8.1	−3.5 ± 6.4	−5.2 ± 2.4	−10.7 ± 2.7	−26.7 ± 4.5 *
18	DF_{high}	42.1 ± 6.4	35.8 ± 5.3	30.3 ± 5.4	−2.9 ± 4.6	−6.2 ± 2.9	−11.7 ± 3.3	−33.2 ± 3.3
	DF_{low}	35.2 ± 8.3	28.8 ± 8.7	23.9 ± 8.6	−4.4 ± 6.7	−6.3 ± 2.8	−11.3 ± 2.8	−28.2 ± 5.0 *
DF groups effect (p)		**<0.001**	**<0.001**	**0.002**	0.248	0.779	0.229	**<0.001**
running speed effect (p)		**<0.001**	**<0.001**	**<0.001**	**<0.001**	**<0.001**	**<0.001**	**<0.001**
interaction effect (p)		0.159	0.399	0.060	0.905	0.516	0.313	**0.012**

Note: data are means ± standard deviation. Angles at foot strike (θ_{FS}), impact attenuation (θ_{IA}), mid-stance (θ_{MS}), and toe-off (θ_{TO}) events together with range of motions during the attenuation ($\Delta\theta_a$), braking ($\Delta\theta_b$), and pushing ($\Delta\theta_p$) phases are presented. Significant differences ($p < 0.05$) identified by the two-way repeated measures ANOVA are indicated in bold. * Significant difference between DF groups at a given speed as determined by Holm post-hoc tests. FS: foot strike, IA: impact attenuation, MS: mid-stance, TO: toe-off, and MF: mid-flight.

Table 4. Knee extension-flexion joint angle at specific events of the running stance (θ_{FS}, θ_{IA}, θ_{MS}, and θ_{TO}) and their range of motions during the different running stance phases ($\Delta\theta_a$, $\Delta\theta_b$, and $\Delta\theta_p$) for the high (DF_{high}) and low (DF_{low}) duty factor running groups at the different running speeds.

Running Speed (km/h)	DF Group	θ_{FS} (deg)	θ_{IA} (deg)	θ_{MS} (deg)	θ_{TO} (deg)	$\Delta\theta_a$ (deg)	$\Delta\theta_b$ (deg)	$\Delta\theta_p$ (deg)
8	DF_{high}	11.9 ± 4.2	24.7 ± 4.6	36.8 ± 4.0	19.2 ± 4.5	12.8 ± 2.1	24.9 ± 4.4	−17.6 ± 3.6
	DF_{low}	13.1 ± 3.5	27.1 ± 4.0	34.8 ± 4.5	18.3 ± 3.9	13.9 ± 2.4	21.7 ± 4.6	−16.5 ± 3.9
10	DF_{high}	11.3 ± 4.1	26.5 ± 4.3	38.2 ± 3.9	19.3 ± 4.9	15.2 ± 2.2	26.9 ± 4.5	−18.9 ± 3.4
	DF_{low}	13.4 ± 3.5	29.2 ± 4.2	36.1 ± 4.4	18.8 ± 4.1	15.8 ± 2.7	22.7 ± 4.8	−17.3 ± 3.8
12	DF_{high}	11.2 ± 4.1	28.3 ± 4.3	39.1 ± 3.5	19.7 ± 4.4	17.0 ± 2.4	27.9 ± 4.1	−19.4 ± 3.1
	DF_{low}	13.2 ± 3.9	30.5 ± 4.7	36.8 ± 4.2	19.0 ± 3.8	17.2 ± 3.1	23.5 ± 4.8	−17.7 ± 3.8
14	DF_{high}	11.8 ± 3.9	30.6 ± 4.3	40.0 ± 4.0	20.1 ± 4.7	18.8 ± 2.6	28.2 ± 4.3	−19.9 ± 3.0
	DF_{low}	13.4 ± 4.1	32.0 ± 4.7	37.5 ± 4.1	19.9 ± 3.7	18.6 ± 3.2	24.1 ± 4.9	−17.7 ± 3.7
16	DF_{high}	12.5 ± 3.5	32.6 ± 4.2	40.7 ± 3.7	20.4 ± 4.6	20.1 ± 2.6	28.2 ± 3.7	−20.3 ± 3.1
	DF_{low}	13.6 ± 4.0	33.2 ± 4.7	37.8 ± 4.2	20.3 ± 3.6	19.6 ± 3.3	24.2 ± 4.7	−17.5 ± 4.0
18	DF_{high}	13.5 ± 3.5	34.4 ± 4.1	41.1 ± 4.1	20.9 ± 4.6	20.9 ± 3.0	27.6 ± 4.1	−20.2 ± 2.8
	DF_{low}	14.0 ± 3.6	34.3 ± 4.4	38.2 ± 4.3	21.1 ± 3.3	20.3 ± 3.5	24.2 ± 4.9	−17.2 ± 4.3
DF groups effect (p)		0.123	0.159	**0.019**	0.717	0.886	**<0.001**	**0.019**
running speed effect (p)		**0.001**	**<0.001**	**<0.001**	**<0.001**	**<0.001**	**<0.001**	**<0.001**
interaction effect (p)		0.139	**0.001**	0.362	0.301	**0.003**	0.410	**0.029**

Note: data are means ± standard deviation. Angles at foot strike (θ_{FS}), impact attenuation (θ_{IA}), mid-stance (θ_{MS}), and toe-off (θ_{TO}) events together with range of motions during the attenuation ($\Delta\theta_a$), braking ($\Delta\theta_b$), and pushing ($\Delta\theta_p$) phases are presented. Significant differences ($p < 0.05$) identified by the two-way repeated measures ANOVA are indicated in bold. No significant difference between DF groups at a given speed was determined by Holm post-hoc tests. FS: foot strike, IA: impact attenuation, MS: mid-stance, TO: toe-off, and MF: mid-flight.

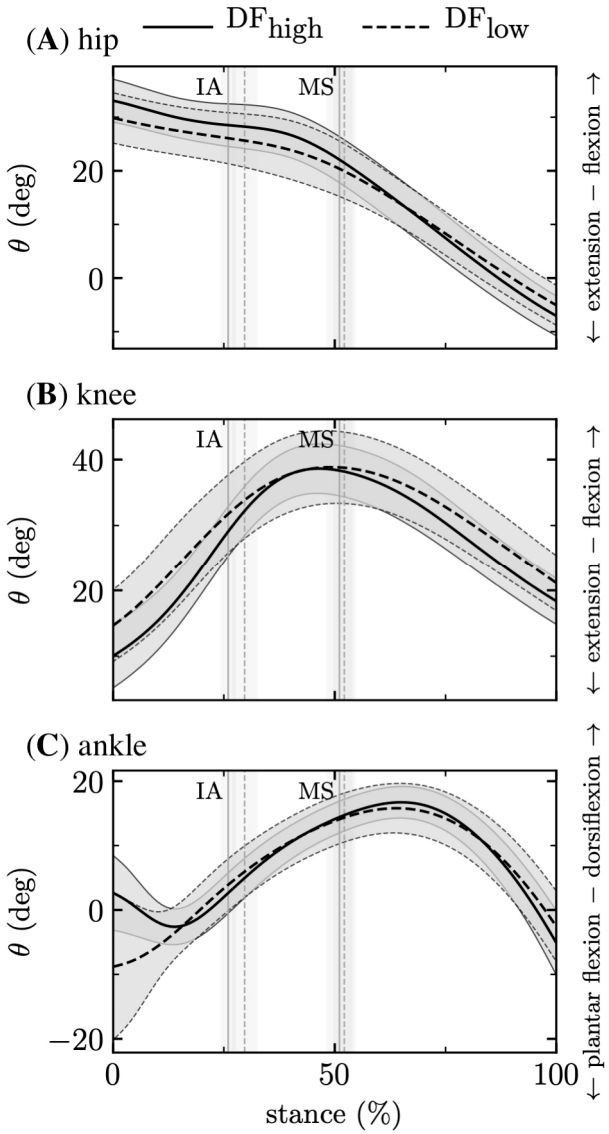

Figure 2. Extension–flexion of the joint angles (θ) during the running stance for the high (DF_{high}) and low (DF_{low}) duty factor running groups while running at 14 km/h for (**A**) hip, (**B**) knee, and (**C**) ankle joint angle. The running speed is representative of all speed. IA: impact attenuation and MS: mid-stance.

A larger plantar flexion was observed at FS for DF_{low} than for DF_{high} (DF groups main effect, $p < 0.001$; large effect size, $d = 1.39$; Table 5 and Figure 2C). DF_{low} exhibited more dorsiflexion during t_a and t_b (larger $\Delta\theta_a$ and $\Delta\theta_b$) than DF_{high} (DF groups main effect, $p < 0.001$; large effect size, $d \geq 1.24$; Table 5 and Figure 2C). The attenuation phase was composed of a plantar flexion followed by a dorsiflexion for DF_{high} whereas it only consisted in an ankle dorsiflexion for DF_{low} (Figure 2C). Running speed affected all ankle angle parameters except $\Delta\theta_b$, with an increase of the plantar flexion at FS and MS and of the dorsiflexion at IA and TO, together with more dorsiflexion during t_a (larger $\Delta\theta_a$) and less plantar flexion during t_p with increasing running speed (smaller $|\Delta\theta_p|$; speed main effect, $p \leq 0.046$; Table 5).

Table 5. Ankle extension–flexion joint angle at specific events of the running stance (θ_{FS}, θ_{IA}, θ_{MS}, and θ_{TO}) and their range of motions during the different running stance phases ($\Delta\theta_a$, $\Delta\theta_b$, and $\Delta\theta_p$) for the high (DF_{high}) and low (DF_{low}) duty factor running groups at the different running speeds.

Running Speed (km/h)	DF Group	θ_{FS} (deg)	θ_{IA} (deg)	θ_{MS} (deg)	θ_{TO} (deg)	$\Delta\theta_a$ (deg)	$\Delta\theta_b$ (deg)	$\Delta\theta_p$ (deg)
8	DF_{high}	−14.8 ± 6.0	−13.5 ± 4.2	−1.5 ± 3.6	−23.3 ± 5.8	1.4 ± 7.0	13.3 ± 5.4	−21.8 ± 4.9
	DF_{low}	−26.9 ± 9.1	−13.1 ± 3.7	−3.1 ± 3.3	−22.7 ± 4.9	13.8 ± 9.7	23.8 ± 9.1	−19.6 ± 4.5
10	DF_{high}	−13.5 ± 5.6	−13.8 ± 4.1	−1.3 ± 3.5	−22.6 ± 5.6	−0.3 ± 6.5	12.3 ± 4.9	−21.3 ± 4.9
	DF_{low}	−26.8 ± 10.1	−12.6 ± 3.8	−2.9 ± 3.4	−21.6 ± 5.3	14.2 ±11.4	23.8 ± 10.3	−18.6 ± 4.8
12	DF_{high}	−13.1 ± 5.3	−14.0 ± 4.3	−1.4 ± 3.6	−21.9 ± 5.8	−0.9 ± 6.3	11.7 ± 4.9	−20.5 ± 4.8
	DF_{low}	−26.4 ± 10.7	−12.5 ± 4.1	−3.1 ± 3.5	−21.2 ± 5.4	13.9 ± 12.5	23.3 ± 11.2	−18.1 ± 4.8
14	DF_{high}	−13.5 ± 6.4	−13.5 ± 4.3	−1.7 ± 3.8	−21.3 ± 5.9	0.0 ± 7.2	11.8 ± 5.7	−19.5 ± 4.8
	DF_{low}	−26.5 ± 10.8	−12.1 ± 4.1	−3.4 ± 3.4	−20.3 ± 5.6	14.5 ± 13.0	23.2 ± 11.0	−16.9 ± 5.0
16	DF_{high}	−14.0 ± 7.1	−12.7 ± 4.4	−2.0 ± 3.9	−20.7 ± 6.1	1.3 ± 7.5	12.0 ± 6.3	−18.7 ± 5.0
	DF_{low}	−27.4 ± 10.9	−11.5 ± 4.2	−3.8 ± 3.6	−19.9 ± 6.0	15.9 ± 13.0	23.6 ± 11.0	−16.0 ± 5.2
18	DF_{high}	−14.9 ± 7.7	−11.6 ± 4.5	−2.5 ± 4.2	−19.8 ± 6.4	3.2 ± 7.7	12.4 ± 6.4	−17.4 ± 4.7
	DF_{low}	−28.2 ± 11.2	−10.8 ± 4.1	−4.3 ± 3.7	−19.7 ± 6.4	17.4 ± 12.9	23.9 ± 10.7	−15.3 ± 5.4
DF groups effect (p)		**<0.001**	0.287	0.069	0.628	**<0.001**	**<0.001**	0.055
running speed effect (p)		**0.046**	**<0.001**	**<0.001**	**<0.001**	**<0.001**	0.317	**<0.001**
interaction effect (p)		0.682	0.190	0.741	0.455	0.438	0.778	0.486

Note: data are means ± standard deviation. Angles at foot strike (θ_{FS}), impact attenuation (θ_{IA}), mid-stance (θ_{MS}), and toe-off (θ_{TO}) events together with range of motions during the attenuation ($\Delta\theta_a$), braking ($\Delta\theta_b$), and pushing ($\Delta\theta_p$) phases are presented. Significant differences ($p < 0.05$) identified by the two-way repeated measures ANOVA are indicated in bold. No significant difference between DF groups at a given speed was determined by Holm post-hoc tests. FS: foot strike, IA: impact attenuation, MS: mid-stance, TO: toe-off, and MF: mid-flight.

3.4. Pelvis and Foot Segment Angles

DF_{high} had a larger pelvis anteversion than DF_{low} at FS (DF groups main effect, $p = 0.026$; medium effect size, $d = 0.53$; Table 6 and Figure 3A). More pelvis retroversion during t_a and t_b (larger $|\Delta\theta_a|$ and $|\Delta\theta_b|$) were observed for DF_{high} (DF groups main effect, $p \leq 0.002$; medium effect size, $d \geq 0.62$; Table 6 and Figure 3A). Running speed affected all pelvis anteversion–retroversion parameters, with an increase of the pelvis anteversion at FS, IA, MS, and TO, less retroversion during t_a and t_b (smaller $|\Delta\theta_a|$ and $|\Delta\theta_b|$), and less anteversion during t_p with increasing running speed (smaller $|\Delta\theta_p|$, speed main effect, $p \leq 0.038$; Table 6). An interaction effect between DF groups and speeds was observed for $\Delta\theta_a$, indicating less pronounced pelvis retroversion during t_a (smaller $|\Delta\theta_a|$) with the increase of running speed for both DF groups ($p = 0.001$; Table 6).

Table 6. Retroversion–anteversion of the pelvis segment angle at specific events of the running stance (θ_{FS}, θ_{IA}, θ_{MS}, and θ_{TO}) and their range of motions during the different running stance phases ($\Delta\theta_a$, $\Delta\theta_b$, and $\Delta\theta_p$) for the high (DF_{high}) and low (DF_{low}) duty factor running groups at the different running speeds.

Running Speed (km/h)	DF Group	θ_{FS} (deg)	θ_{IA} (deg)	θ_{MS} (deg)	θ_{TO} (deg)	$\Delta\theta_a$ (deg)	$\Delta\theta_b$ (deg)	$\Delta\theta_p$ (deg)
8	DF_{high}	3.8 ± 3.1	0.7 ± 2.9	−0.7 ± 3.6	2.7 ± 3.1	−3.0 ± 1.1	−4.5 ± 2.0	3.4 ± 1.4
	DF_{low}	2.3 ± 3.3	−0.6 ± 3.0	−0.6 ± 3.4	2.2 ± 3.0	−2.9 ± 1.1	−2.9 ± 1.9	2.9 ± 1.4
10	DF_{high}	4.8 ± 3.4	1.2 ± 3.1	0.5 ± 3.7	3.5 ± 3.2	−3.6 ± 1.2	−4.3 ± 2.2	2.9 ± 1.3
	DF_{low}	2.6 ± 3.4	−0.3 ± 3.1	0.2 ± 3.7	2.6 ± 3.3	−2.9 ± 1.3	−2.5 ± 1.8	2.5 ± 1.5
12	DF_{high}	5.1 ± 3.6	1.2 ± 3.2	1.2 ± 3.7	3.6 ± 3.3	−3.9 ± 1.6	−4.0 ± 2.4	2.5 ± 1.3
	DF_{low}	2.8 ± 3.8	0.2 ± 3.4	0.8 ± 4.0	2.8 ± 3.7	−2.7 ± 1.3	−2.0 ± 1.6	1.9 ± 1.3
14	DF_{high}	4.9 ± 3.6	1.1 ± 3.3	1.6 ± 3.8	3.4 ± 3.4	−3.8 ± 1.9	−3.3 ± 2.6	1.8 ± 1.3
	DF_{low}	2.5 ± 3.9	0.3 ± 3.5	1.2 ± 4.1	2.5 ± 4.1	−2.3 ± 1.3 *	−1.4 ± 1.7	1.4 ± 1.4
16	DF_{high}	4.5 ± 3.5	1.1 ± 3.3	1.9 ± 3.8	3.1 ± 3.6	−3.4 ± 2.1	−2.6 ± 2.8	1.2 ± 1.4
	DF_{low}	2.3 ± 4.1	0.4 ± 4.0	1.3 ± 4.6	2.2 ± 4.4	−1.9 ± 1.3 *	−1.0 ± 1.7	0.8 ± 1.5
18	DF_{high}	4.4 ± 3.6	1.3 ± 3.4	2.3 ± 3.9	2.9 ± 3.9	−3.1 ± 2.5	−2.1 ± 3.1	0.6 ± 1.6
	DF_{low}	2.3 ± 4.6	0.8 ± 4.5	1.7 ± 5.0	2.0 ± 4.8	−1.5 ± 1.5 *	−0.7 ± 1.8	0.3 ± 1.4
DF groups effect (p)		**0.026**	0.243	0.700	0.368	**0.004**	**0.002**	0.193
running speed effect (p)		**0.019**	**0.010**	**<0.001**	**0.038**	**<0.001**	**<0.001**	**<0.001**
interaction effect (p)		0.318	0.197	0.508	0.700	**0.001**	0.394	0.660

Note: data are means ± standard deviation. Segment angles at foot strike (θ_{FS}), impact attenuation (θ_{IA}), mid-stance (θ_{MS}), and toe-off (θ_{TO}) events together with range of motions during the attenuation ($\Delta\theta_a$), braking ($\Delta\theta_b$), and pushing ($\Delta\theta_p$) phases are presented. Segment angles are expressed as a difference with respect to segment angles in static upright stance. Significant differences ($p < 0.05$) identified by the two-way repeated measures ANOVA are indicated in bold. * Significant difference between DF groups at a given speed as determined by Holm post-hoc tests. FS: foot strike, IA: impact attenuation, MS: mid-stance, TO: toe-off, MF: mid-flight, and NA: not-applicable.

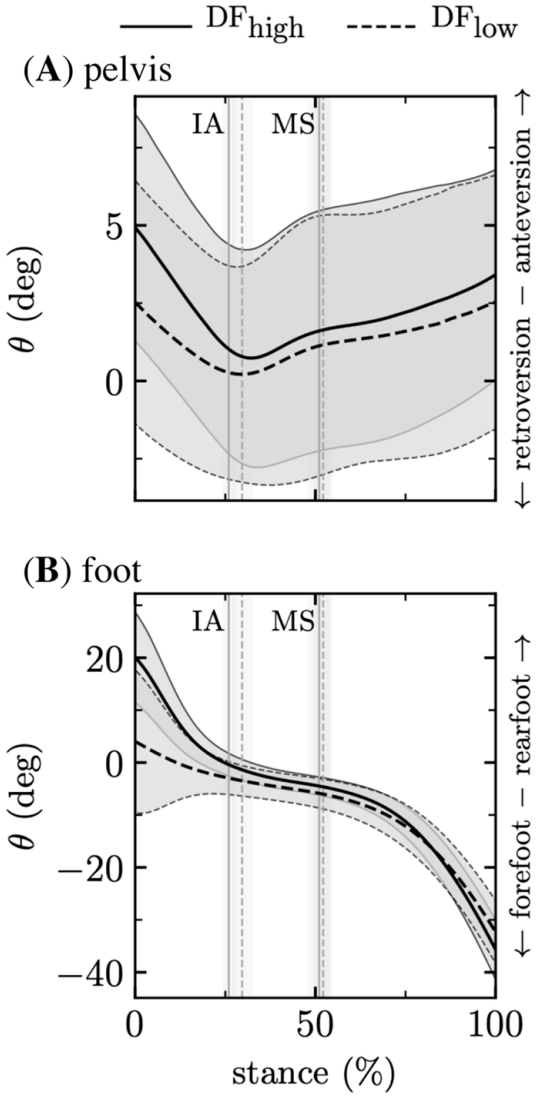

Figure 3. Segment angles (θ) during the running stance for the high (DF$_{high}$) and low (DF$_{low}$) duty factor running groups while running at 14 km/h for (**A**) pelvis (retroversion-anteversion) and (**B**) foot (forefoot–rearfoot) segment angle, expressed as a difference with respect to segment angle in the static upright stance. The running speed is representative of all speed. IA: impact attenuation, MS: mid-stance, rot: rotation.

DF$_{high}$ had a more pronounced rearfoot angle at FS and IA, a smaller forefoot angle at MS, and a larger forefoot angle at TO than DF$_{low}$ (DF groups main effect, $p \leq 0.028$; θ_{FS} and θ_{IA}: large effect size, $d \geq 1.10$; θ_{MS} and θ_{TO}: medium effect size, $d \geq 0.60$; Table 7 and Figure 3B). More forefoot angle during t_a, t_b, and t_p (larger $|\Delta\theta_a|$, $|\Delta\theta_b|$, and $|\Delta\theta_p|$) were observed for DF$_{high}$ (DF groups main effect, $p < 0.001$; large effect size, $d \geq 1.04$; Table 7 and Figure 3B). Running speed affected all forefoot–rearfoot angle parameters, with an increase of the rearfoot angle at FS, an increase of the forefoot angle at IA, MS, and TO, and more forefoot angle during t_a, t_b, and t_p with increasing running speed (larger $|\Delta\theta_a|$, $|\Delta\theta_b|$, and $|\Delta\theta_p|$; speed main effect, $p \leq 0.001$; Table 7). The interaction effect indicated a slight increase of the forefoot angle at IA with the increase of running speed for both DF groups ($p = 0.001$; Table 7).

Table 7. Forefoot–rearfoot of the foot segment angle at specific events of the running stance (θ_{FS}, θ_{IA}, θ_{MS}, and θ_{TO}) and their range of motions during the different running stance phases ($\Delta\theta_a$, $\Delta\theta_b$, and $\Delta\theta_p$) for the high (DF_{high}) and low (DF_{low}) duty factor running groups at the different running speeds.

Running Speed (km/h)	DF Group	θ_{FS} (deg)	θ_{IA} (deg)	θ_{MS} (deg)	θ_{TO} (deg)	$\Delta\theta_a$ (deg)	$\Delta\theta_b$ (deg)	$\Delta\theta_p$ (deg)
8	DF_{high}	12.2 ± 8.4	0.5 ± 2.5	−3.7 ± 1.6	−32.4 ± 5.3	−11.7 ± 6.4	−15.9 ± 7.8	−28.6 ± 5.3
	DF_{low}	−2.4 ± 10.5	−3.3 ± 3.1 *	−5.1 ± 2.2	−29.3 ± 5.0	−1.0 ± 8.2	−2.8 ± 9.4	−24.1 ± 4.0
10	DF_{high}	16.3 ± 8.2	0.6 ± 2.4	−4.0 ± 1.6	−33.9 ± 5.3	−15.7 ± 6.3	−20.2 ± 7.7	−29.9 ± 5.2
	DF_{low}	−0.1 ± 11.8	−3.2 ± 2.9 *	−5.4 ± 2.4	−30.2 ± 5.7	−3.1 ± 9.6	−5.3 ± 10.7	−24.8 ± 4.5
12	DF_{high}	19.0 ± 7.9	0.4 ± 2.3	−4.2 ± 1.6	−35.0 ± 5.4	−18.6 ± 6.1	−23.1 ± 7.2	−30.9 ± 5.1
	DF_{low}	2.2 ± 12.9	−3.2 ± 3.0 *	−5.6 ± 2.6	−31.6 ± 5.7	−5.4 ± 10.6	−7.9 ± 11.5	−25.9 ± 4.4
14	DF_{high}	20.1 ± 8.6	−0.3 ± 2.2	−4.5 ± 1.8	−35.7 ± 5.7	−20.4 ± 6.9	−24.6 ± 7.8	−31.2 ± 5.3
	DF_{low}	4.0 ± 13.6	−3.3 ± 3.1 *	−6.0 ± 2.9	−32.4 ± 6.0	−7.4 ± 11.3	−10.1 ± 12.3	−26.3 ± 4.5
16	DF_{high}	20.6 ± 8.8	−0.9 ± 2.2	−4.7 ± 1.9	−36.4 ± 5.6	−21.5 ± 7.2	−25.3 ± 7.9	−31.7 ± 5.1
	DF_{low}	4.6 ± 13.9	−3.6 ± 3.2 *	−6.2 ± 3.2	−33.0 ± 6.3	−8.2 ± 11.5	−10.9 ± 12.2	−26.7 ± 4.7
18	DF_{high}	20.6 ± 8.5	−1.4 ± 2.2	−4.8 ± 2.0	−36.5 ± 5.6	−22.0 ± 7.1	−25.5 ± 7.8	−31.7 ± 4.9
	DF_{low}	5.1 ± 14.2	−3.9 ± 3.3 *	−6.5 ± 3.2	−33.9 ± 6.8	−9.0 ± 11.9	−11.5 ± 12.7	−27.4 ± 5.1
DF groups effect (p)		**<0.001**	**<0.001**	**0.012**	**0.028**	**<0.001**	**<0.001**	**<0.001**
running speed effect (p)		**<0.001**	**<0.001**	**<0.001**	**<0.001**	**<0.001**	**<0.001**	**<0.001**
interaction effect (p)		0.558	**0.001**	0.623	0.376	0.265	0.542	0.416

Note: data are means ± standard deviation. Segment angles at foot strike (θ_{FS}), impact attenuation (θ_{IA}), mid-stance (θ_{MS}), and toe-off (θ_{TO}) events together with range of motions during the attenuation ($\Delta\theta_a$), braking ($\Delta\theta_b$), and pushing ($\Delta\theta_p$) phases are presented. Segment angles are expressed as a difference with respect to segment angles in static upright stance. Significant differences ($p < 0.05$) identified by the two-way repeated measures ANOVA are indicated in bold. * Significant difference between DF groups at a given speed as determined by Holm post-hoc tests. FS: foot strike, IA: impact attenuation, MS: mid-stance, TO: toe-off, MF: mid-flight, and NA: not applicable.

3.5. Running Wheel

The running wheel at 14 km/h was more vertical for DF_{low} (maximum of the vertical position of the center of mass of the foot segment, i.e., z_{foot} = 50%) than for DF_{high} (maximum of z_{foot} = 40%; Figure 4). The antero-posterior range of motion of the running wheel was similar between both DF groups at 14 km/h (range of motion = 107%; Figure 4). However, DF_{high} had a smaller minimum posterior position of the foot at 14 km/h (minimum of the antero-posterior position of the center of mass of the foot segment, i.e., y_{foot} = –96%) compared to DF_{low} (minimum of y_{foot} = –102%; Figure 4). The compensation happened right before the foot struck the ground with a larger maximum anterior position of the foot for DF_{low} (maximum z_{foot} = 9%) than for DF_{high} (maximum y_{foot} = 5%; Figure 4) at 14 km/h. Similar effects were observed at all speeds with a more pronounced difference at a higher speed.

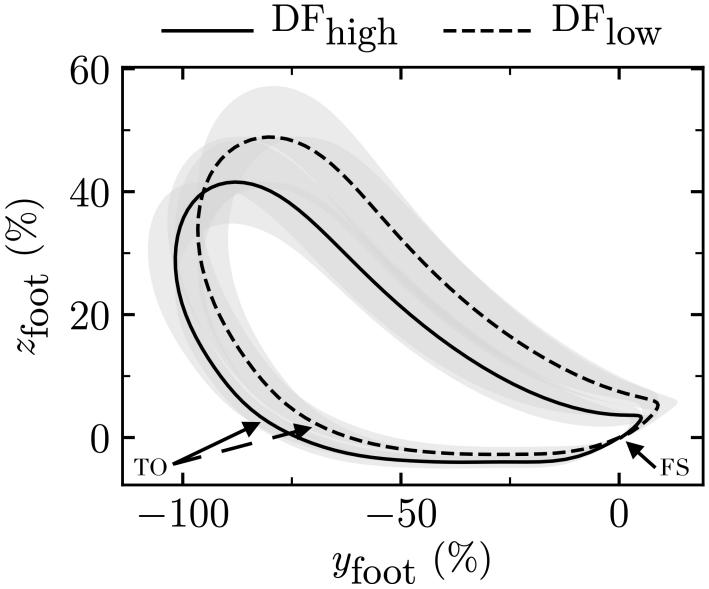

Figure 4. Running wheel for the high (DF_{high}) and low (DF_{low}) duty factor running groups while running at 14 km/h. The running wheel is defined as the vertical versus antero-posterior position of the center of mass of the foot segment, expressed as a percentage of participant's leg length. Position (0, 0) defines the point where the center of mass of the foot segment strikes the ground. FS: foot strike and TO: toe-off.

4. Discussion

In this study, in accordance with our hypothesis, DF_{high} was relying on more lower limb flexion during t_c than DF_{low} despite a similar knee flexion at FS. In addition, DF_{high} was striking the ground using the rearfoot while the midfoot was used in DF_{low}. These two DF groups allow one to distinguish between two lower limb kinematic mechanisms in running.

The DF values in our sample of runners (Table 1) were similar to those previously reported in the literature at similar running speeds and agree with the fact that DF values of running locomotion should be under 50.0% [17,54,60]. DF_{low} exhibited significantly shorter t_b and t_p but longer t_e and t_d associated with larger $\Delta z_{COM,e}$ and $\Delta z_{COM,d}$ than DF_{high} (Table 2). In addition, with increasing running speed, DF_{high} was more prone to decrease t_b and t_p and to increase t_e and t_d than DF_{low} (Table 2). Increasing the running speed leads to the decrease of t_c and increase of t_f. Therefore, as DF_{high} runners start from larger t_c and smaller t_f at 8 km/h than DF_{low} and as t_c and t_f cannot indefinitely decrease and increase, respectively, the observed results naturally follow. These findings are in agreement with the observations of Lussiana et al. (2019). The running wheel was more vertical for DF_{low} than DF_{high} while the antero-posterior range of motion was similar between groups (Figure 4). However, DF_{low} was shown to use a more anterior running wheel than DF_{high} while DF_{high}

a more posterior one than DF_{low} (Figure 4). These different running wheels are reflecting the different temporal characteristics and COM displacements between the DF groups. As DF_{low} depicted larger t_d and $\Delta z_{COM,d}$ than DF_{high}, their vertical speed and thus vertical kinetic energy was higher at impact. In addition, the smaller t_b and t_p and therefore t_c observed in DF_{low} are indications that these runners have a presumably higher stiffness of the lower limb than DF_{high} [61]. These observations led to the idea that DF_{low} relies on the reuse of elastic energy (optimization of the spring-mass model) while DF_{high} limits vertical displacement of the COM and promote forward propulsion (pulley system) to minimize running economy [17]. Similar conclusions were drawn when classifying runners based on a subjective evaluation of the spontaneous overall running pattern [19]. Besides a different strategy to minimize running economy between these two DF groups, these differences in running biomechanics also suggest different lower limb kinematic mechanisms.

Following the classification of FS pattern proposed by Altman and Davis (2012), DF_{high} exhibited a rearfoot strike pattern [62] at FS while DF_{low} was midfoot strikers (Table 7). The fact that DF_{low} did not show a clear forefoot strike pattern is probably related to the fact almost 90% of the population is striking the ground with the rearfoot [63] and that the inclusion criteria of this study were not specifically based on the strike pattern. Nevertheless, taken as a group, DF_{low} runners were certainly using more their midfoot and forefoot than DF_{high} (Table 7). Accordingly, a significantly more pronounced forefoot angle was observed at IA and MS for DF_{low} than DF_{high}, suggesting that DF_{high} is relying more on the rearfoot during t_a and t_b than DF_{low}. This is also partly explaining why the foot segment angle is not exactly zero at MS. Indeed, the body, and especially the foot, is applying a higher force to the ground during the ground contact phase of the running stride than when standing in a static upright stance, leading to more compression in the rear (DF_{high}) or fore (DF_{low}) part of the shoe insole and thus providing a non-zero angle. In addition, DF_{high} depicted a significantly larger forefoot angle at TO than DF_{low}, which was associated with a significantly larger $|\Delta\theta_p|$ (Table 7). These findings further suggest that DF_{high} promotes forward propulsion by pushing more with the toes during t_p.

DF_{low} exhibited significantly more plantar flexion at FS and more dorsiflexion during t_a and t_b than DF_{high} (Table 5). A visual observation of Figure 2C depicts that a plantar flexion takes place at the very first instants of the stance for DF_{high}, right before the usual dorsiflexion. These results suggest that DF_{low} relies on the midfoot to forefoot and the eccentric action of the plantar–flexor muscles to attenuate the impact. On the contrary, DF_{high} seems to additionally rely on the eccentric action of the dorsiflexor muscles, as already pointed out by Breine et al. (2019) for rearfoot strikers. The findings of this study mirror previous observations of rearfoot and forefoot strikers. Indeed, Derrick et al. (1998) observed that rearfoot strikers were absorbing most of the impact shock using the heel and skeletal tissue whereas forefoot strikers used an eccentric action of the plantar flexor muscles to absorb the shock [25,38,39]. Additionally, a rearfoot strike pattern was shown to cause a significant impact force on the heel, whereas peak plantar pressure was centered at the forefoot when forefoot striking [41]. Similarly, Dickinson et al. (1985) mentioned that for forefoot strikers, instead of being primarily an energy producer, the ankle takes the additional task of absorbing energy during t_b and Hasegawa et al. (2007) pointed out the fact that shorter t_c and increased plantar flexion angles require a greater amount of energy to be absorbed at the ankle [64].

When focusing on the entire lower limb, a larger range of hip extension and a greater increase in the range of motion of hip extension with increasing running speed during t_p was observed for DF_{high} than for DF_{low} (Table 4). Besides, DF_{high} demonstrated more hip flexion at FS, IA, and MS (Table 3) but a similar range of motion during t_a and t_b than DF_{low}. In addition, the pelvis showed a higher range of retroversion during t_a and t_b and no change of retroversion with increasing running speed (Table 6) despite a statistically higher anteversion at FS for DF_{high} than DF_{low}. The lower vertical kinetic energy at impact (shorter t_d and smaller $\Delta z_{COM,d}$) and thus a softer (less stiff) lower limb allows a higher pelvis mobility in DF_{high} than DF_{low} and to rotate in the three anatomical planes (see Supplementary Materials) while DF_{low} requires, due to the higher vertical kinetic energy at FS, a stiffer lower limb than DF_{high}, which suggests limiting the rotation in the sagittal plane. Furthermore, less knee flexion

was observed for DF_{low} than DF_{high} at MS but a similar one at FS, which led to a larger range of motion of the knee joint angle during t_b and t_p for DF_{high} than DF_{low} (Table 4). Therefore, a larger leg compression and decompression was observed for DF_{high} than DF_{low} despite the similar knee joint angle at FS. In addition, with increasing running speed, DF_{high} depicted a larger increase of knee flexion at IA than DF_{low} and a larger increase in the range of motion of the knee joint during t_a and t_p (Table 4). These findings are potentially representing a more pronounced eccentric action of the quadriceps muscle for DF_{high} than DF_{low} during t_b. These results are in line with the observations of Gerritsen et al. (1995), which showed that the eccentric action of the knee extensor muscles was playing a role to attenuate the impact when rearfoot striking. Additionally, Knorz et al. (2017) have shown that different FS patterns change the distribution of loadings in a runner's body. The authors concluded that a forefoot strike pattern was generally associated with a greater vertical maximum peak force but significantly lower loading rates in the ankle, knee, and hip joints, which is in line with the lower flexion and compression of the lower limb observed for DF_{low} than DF_{high}. Similar studies were performed by other researchers and demonstrated that a forefoot strike pattern reduces knee loads whereas a rearfoot strike pattern reduces loads at the Achilles tendon [65–67] and ankle joint [68], again agreeing with less lower limb flexion for DF_{low} than DF_{high}.

Running speed affected most of the biomechanical parameters. t_c decreased while t_f increased with the increase of the running speed, leading to higher vertical oscillations of the COM during t_f but smaller ones during t_c for both DF groups. Similar observations were obtained by Lussiana et al. (2019). These results suggest that the increase of the running speed promotes the DF_{low} temporal characteristics and COM displacements rather than the DF_{high} ones, i.e., a faster running speed favors t_f and corresponding COM displacements. However, the hip and knee flexions and the ankle dorsiflexion were increased during t_c with an increase of the running speed for both DF groups. Moreover, a more rearfoot strike pattern was observed for both DF_{high} and DF_{low} with increasing running speed. An increase of the FS angle was also observed for aerial and terrestrial runners with the increase of the running speed [16]. These results suggest more lower limb flexion with increasing running speed. Nevertheless, even if higher running speeds seem to produce a favor to t_f associated with more lower limb flexion during t_c, differences between DF_{low} and DF_{high} are present at all speeds, with DF_{low} showing a higher favor to t_f and a more extended lower limb during t_c than DF_{high}.

Overall, these findings suggest the presence of two different lower limb kinematic mechanisms, which are directly linked to the runner's DF. These two mechanisms could be related to two different impact attenuation strategies. The existence of different type of shock attenuation strategies was already proposed by Novacheck (1998). Indeed, the author related these different strategies to the different forms of impact passive peak on the vertical ground reaction force [69]. A similar impact attenuation strategy than the DF_{high} one was observed for "Groucho" running [45], while the shock absorption for "Pose" running [46] resembles the one of DF_{low}. These two different strategies seem to rely on different muscles, i.e., plantar flexor muscles for DF_{low} and dorsiflexor and quadriceps muscles for DF_{high}. Altogether, it can be speculated that the impact attenuation strategy is also self-selected and is another part of the subconsciously driven self-optimization, a central element in the development of an economical and safe running gait [1,9–11].

A few limitations to the present study exist. The ground reaction forces were not measured, thus making it not possible to directly link the calculated running kinematics (temporal characteristics, COM displacement, and joint and segment angles of the running step) to the impact loadings on the lower limb. Furthermore, whole-body 3D kinematic data was collected in order to report how the body globally structures itself while running. However, this "global" choice limited the precision of our 3D measurements when considering segment angles (as depicted by the large standard deviations). Therefore, further studies should focus on specific segment (and joint) angles to potentially observe more precise details. Moreover, no sex distinction was taken into account within the full-body biomechanical model. More specifically, a male-specific set of body segment parameters was used in Visual3D [48,49], which could have impacted the outcomes, such as the COM, and could have

confounded conclusions. In addition, no sex distinction was taken into account within our DF groups. Thus, future work should focus on the impact of sex on global running pattern. For instance, one could wonder if, within a DF group, females depict similar lower limb flexion than males. Finally, FS and TO events were defined from an algorithm which has not yet been validated. However, all events were verified to ensure correct identification and were manually adjusted when required. Nonetheless, a future study focusing on the validation of this algorithm should be conducted to avoid manual verification of all events.

5. Conclusions

To conclude, this study observed that two lower limb kinematic mechanisms were involved in running and the one of an individual is reflected by the DF. DF_{low} runners were shown to exhibit a more extended lower limb than DF_{high} due to a stiffer leg, which requires less range of motion at the knee and hip joints, and to be midfoot and forefoot strikers. On the contrary, DF_{high} runners, which limit vertical displacement of the COM and promote forward propulsion, exhibited more lower limb flexion during t_c than DF_{low} and were rearfoot strikers.

Supplementary Materials: The supplementary materials are available online at http://www.mdpi.com/2076-3417/10/24/8818/s1.

Author Contributions: Conceptualization, T.L. and C.G.; methodology, T.L., L.M., and C.G.; investigation, T.L. and A.T.; formal analysis, A.P.; writing—original draft preparation, A.P.; writing—review and editing, A.P., T.L., A.T., L.M., and C.G.; supervision, L.M. and C.G. All authors have read and agreed to the published version of the manuscript.

Funding: This research did not receive any specific grant from funding agencies in the public, commercial, or not-for-profit sectors.

Acknowledgments: This study was supported by the University of Lausanne, the Volodalen company, the University of Franche-Comté, and Tomsk Polytechnic University CE Program. The authors warmly thank the participants for their time and cooperation.

Conflicts of Interest: The authors declare no conflict of interest.

References

1. Cavanagh, P.R.; Williams, K.R. The effect of stride length variation on oxygen uptake during distance running. *Med. Sci. Sports Exerc.* **1982**, *14*, 30–35. [CrossRef]
2. Connick, M.J.; Li, F.-X. Changes in timing of muscle contractions and running economy with altered stride pattern during running. *Gait Posture* **2014**, *39*, 634–637. [CrossRef] [PubMed]
3. de Ruiter, C.J.; Verdijk, P.W.L.; Werker, W.; Zuidema, M.J.; de Haan, A. Stride frequency in relation to oxygen consumption in experienced and novice runners. *Eur. J. Sport Sci.* **2014**, *14*, 251–258. [CrossRef]
4. Högberg, P. How do stride length and stride frequency influence the energy-output during running? *Arbeitsphysiologie* **1952**, *14*, 437–441. [CrossRef] [PubMed]
5. Hunter, I.; Smith, G.A. Preferred and optimal stride frequency, stiffness and economy: Changes with fatigue during a 1-h high-intensity run. *Eur. J. Appl. Physiol.* **2007**, *100*, 653–661. [CrossRef] [PubMed]
6. Morgan, D.; Martin, P.; Craib, M.; Caruso, C.; Clifton, R.; Hopewell, R. Effect of step length optimization on the aerobic demand of running. *J. Appl. Physiol. Bethesda* **1994**, *77*, 245–251. [CrossRef]
7. Van Oeveren, B.T.; de Ruiter, C.J.; Beek, P.J.; van Dieën, J.H. Optimal stride frequencies in running at different speeds. *PLoS ONE* **2017**, *12*, e0184273. [CrossRef]
8. Moore, I.S.; Ashford, K.J.; Cross, C.; Hope, J.; Jones, H.S.R.; McCarthy-Ryan, M. Humans optimize ground contact time and leg stiffness to minimize the metabolic cost of running. *Front. Sports Act. Living* **2019**, *1*. [CrossRef]
9. Williams, K.R.; Cavanagh, P.R. Relationship between distance running mechanics, running economy, and performance. *J. Appl. Physiol. Bethesda* **1987**, *63*, 1236–1245. [CrossRef]
10. Moore, I.S.; Jones, A.M.; Dixon, S.J. Mechanisms for improved running economy in beginner runners. *Med. Sci. Sports Exerc.* **2012**, *44*, 1756–1763. [CrossRef]

11. Moore, I.S.; Jones, A.M.; Dixon, S.J. Reduced oxygen cost of running is related to alignment of the resultant GRF and leg axis vector: A pilot study. *Scand. J. Med. Sci. Sports* **2016**, *26*, 809–815. [CrossRef] [PubMed]
12. Williams, K.R. Biomechanical factors contributing to marathon race success. *Sports Med.* **2007**, *37*, 420–423. [CrossRef] [PubMed]
13. Hoerzer, S.; von Tscharner, V.; Jacob, C.; Nigg, B.M. Defining functional groups based on running kinematics using self-organizing maps and support vector machines. *J. Biomech.* **2015**, *48*, 2072–2079. [CrossRef] [PubMed]
14. Phinyomark, A.; Osis, S.; Hettinga, B.A.; Ferber, R. Kinematic gait patterns in healthy runners: A hierarchical cluster analysis. *J. Biomech.* **2015**, *48*, 3897–3904. [CrossRef]
15. Gindre, C.; Lussiana, T.; Hebert-Losier, K.; Mourot, L. Aerial and Terrestrial patterns: A novel approach to analyzing human running. *Int. J. Sports Med.* **2016**, *37*, 25–29. [CrossRef]
16. Lussiana, T.; Gindre, C.; Mourot, L.; Hébert-Losier, K. Do subjective assessments of running patterns reflect objective parameters? *Eur. J. Sport Sci.* **2017**, *17*, 847–857. [CrossRef]
17. Lussiana, T.; Patoz, A.; Gindre, C.; Mourot, L.; Hébert-Losier, K. The implications of time on the ground on running economy: Less is not always better. *J. Exp. Biol.* **2019**, *222*. [CrossRef]
18. Patoz, A.; Gindre, C.; Thouvenot, A.; Mourot, L.; Hébert-Losier, K.; Lussiana, T. Duty factor is a viable measure to classify spontaneous running forms. *Sports* **2019**, *7*, 233. [CrossRef]
19. Lussiana, T.; Gindre, C.; Hébert-Losier, K.; Sagawa, Y.; Gimenez, P.; Mourot, L. Similar running economy with different running patterns along the aerial-terrestrial continuum. *Int. J. Sports Physiol. Perform.* **2017**, *12*, 481–489. [CrossRef]
20. Forrester, S.E.; Townend, J. The effect of running velocity on footstrike angle-a curve-clustering approach. *Gait Posture* **2015**, *41*, 26–32. [CrossRef]
21. Craighead, D.H.; Lehecka, N.; King, D.L. A novel running mechanic's class changes kinematics but not running economy. *J. Strength Cond. Res.* **2014**, *28*, 3137–3145. [CrossRef] [PubMed]
22. Hamill, J.; Gruber, A.H. Is changing footstrike pattern beneficial to runners? *J. Sport Health Sci.* **2017**, *6*, 146–153. [CrossRef] [PubMed]
23. Ekizos, A.; Santuz, A.; Arampatzis, A. Short- and long-term effects of altered point of ground reaction force application on human running energetics. *J. Exp. Biol.* **2018**, *221*, 1–15. [CrossRef]
24. Derrick, T.R.; Hamill, J.; Caldwell, G.E. Energy absorption of impacts during running at various stride lengths. *Med. Sci. Sports Exerc.* **1998**, *30*, 128–135. [CrossRef] [PubMed]
25. Laughton, C.A.; Davis, I.; Hamill, J. Effect of strike pattern and orthotic intervention on tibial shock during running. *J. Appl. Biomech.* **2003**, *19*, 153–168. [CrossRef]
26. Cavanagh, P.R.; Lafortune, M.A. Ground reaction forces in distance running. *J. Biomech.* **1980**, *13*, 397–406. [CrossRef]
27. Dickinson, J.A.; Cook, S.D.; Leinhardt, T.M. The measurement of shock waves following heel strike while running. *J. Biomech.* **1985**, *18*, 415–422. [CrossRef]
28. Munro, C.F.; Miller, D.I.; Fuglevand, A.J. Ground reaction forces in running: A reexamination. *J. Biomech.* **1987**, *20*, 147–155. [CrossRef]
29. Nigg, B.M.; Cole, G.K.; Brüggemann, G.-P. Impact forces during heel-toe running. *J. Appl. Biomech.* **1995**, *11*, 407–432. [CrossRef]
30. Derrick, T.R.; Knight, C.; Heiderscheit, B.; Hamill, J. Spectral decomposition of vertical ground reaction force curves. *ISBS Conf. Proc. Arch.* **1996**.
31. Nigg, B.M.; Wakeling, J.M. Impact forces and muscle tuning: A new paradigm. *Exerc. Sport Sci. Rev.* **2001**, *29*, 37–41. [CrossRef] [PubMed]
32. Breine, B.; Malcolm, P.; Segers, V.; Gerlo, J.; Derie, R.; Pataky, T.; Frederick, E.C.; De Clercq, D. Magnitude and spatial distribution of impact intensity under the foot relates to initial foot contact pattern. *J. Appl. Biomech.* **2017**, *33*, 431–436. [CrossRef] [PubMed]
33. Breine, B.; Malcolm, P.; Van Caekenberghe, I.; Fiers, P.; Frederick, E.C.; De Clercq, D. Initial foot contact and related kinematics affect impact loading rate in running. *J. Sports Sci.* **2017**, *35*, 1556–1564. [CrossRef] [PubMed]
34. Gruber, A.H.; Boyer, K.A.; Derrick, T.R.; Hamill, J. Impact shock frequency components and attenuation in rearfoot and forefoot running. *J. Sport Health Sci.* **2014**, *3*, 113–121. [CrossRef]

35. Gruber, A.H.; Davis, I.S.; Hamill, J. Frequency content of the vertical ground reaction force component during rearfoot and forefoot running patterns. *Med. Sci. Sports Exerc.* **2011**, *43*, 60. [CrossRef]
36. Breine, B.; Malcolm, P.; Galle, S.; Fiers, P.; Frederick, E.C.; De Clercq, D. Running speed-induced changes in foot contact pattern influence impact loading rate. *Eur. J. Sport Sci.* **2019**, *19*, 774–783. [CrossRef] [PubMed]
37. Gerritsen, K.G.; van den Bogert, A.J.; Nigg, B.M. Direct dynamics simulation of the impact phase in heel-toe running. *J. Biomech.* **1995**, *28*, 661–668. [CrossRef]
38. Pratt, D.J. Mechanisms of shock attenuation via the lower extremity during running. *Clin. Biomech.* **1989**, *4*, 51–57. [CrossRef]
39. Williams, D.S.; McClay, I.S.; Manal, K.T. Lower extremity mechanics in runners with a converted forefoot strike pattern. *J. Appl. Biomech.* **2000**, *16*, 210–218. [CrossRef]
40. Knorz, S.; Kluge, F.; Gelse, K.; Schulz-Drost, S.; Hotfiel, T.; Lochmann, M.; Eskofier, B.; Krinner, S. Three-dimensional biomechanical analysis of rearfoot and forefoot running. *Orthop. J. Sports Med.* **2017**, *5*, 2325967117719065. [CrossRef]
41. Sun, X.; Yang, Y.; Wang, L.; Zhang, X.; Fu, W. Do strike patterns or shoe conditions have a predominant influence on foot loading? *J. Hum. Kinet.* **2018**, *64*, 13–23. [CrossRef] [PubMed]
42. Anderson, L.M.; Bonanno, D.R.; Hart, H.F.; Barton, C.J. What are the benefits and risks associated with changing foot strike pattern during running? A systematic review and meta-analysis of injury, running economy, and biomechanics. *Sports Med.* **2019**. [CrossRef] [PubMed]
43. Almeida, M.O.; Davis, I.S.; Lopes, A.D. Biomechanical differences of foot-strike patterns during running: A systematic review with meta-analysis. *J. Orthop. Sports Phys. Ther.* **2015**, *45*, 738–755. [CrossRef] [PubMed]
44. Ó'Catháin, C.P.; Richter, C.; Moran, K. Can directed compliant running reduce the magnitude of variables associated with the development of running injuries? *J. Strength Cond. Res.* **2020**. [CrossRef]
45. McMahon, T.A.; Valiant, G.; Frederick, E.C. Groucho running. *J. Appl. Physiol.* **1987**, *62*, 2326–2337. [CrossRef] [PubMed]
46. Arendse, R.E.; Noakes, T.D.; Azevedo, L.B.; Romanov, N.; Schwellnus, M.P.; Fletcher, G. Reduced eccentric loading of the knee with the pose running method. *Med. Sci. Sports Exerc.* **2004**, *36*, 272–277. [CrossRef] [PubMed]
47. Tranberg, R.; Saari, T.; Zügner, R.; Kärrholm, J. Simultaneous measurements of knee motion using an optical tracking system and radiostereometric analysis (RSA). *Acta Orthop.* **2011**, *82*, 171–176. [CrossRef] [PubMed]
48. Hanavan, E. A mathematical model of the human body. *AMRL-TR Aerosp. Med. Res. Lab.* **1964**, *1*, 1–149.
49. Dempster, W.T. *Space Requirements of the Seated Operator: Geometrical, Kinematic, and Mechanical Aspects of the Body with Special Reference to the Limbs*; Wright Air Development Center, Wright-Patterson Air Force Base: Montgomery County, OH, USA, 1955.
50. Woltring, H. Representation and calculation of 3-D joint movement. *Hum. Mov. Sci.* **1991**, *10*, 603–616. [CrossRef]
51. Davis, R.B.; Õunpuu, S.; Tyburski, D.; Gage, J.R. A gait analysis data collection and reduction technique. *Hum. Mov. Sci.* **1991**, *10*, 575–587. [CrossRef]
52. Cole, G.K.; Nigg, B.M.; Ronsky, J.L.; Yeadon, M.R. Application of the joint coordinate system to three-dimensional joint attitude and movement representation: A standardization proposal. *J. Biomech. Eng.* **1993**, *115*, 344–349. [CrossRef] [PubMed]
53. Grood, E.S.; Suntay, W.J. A joint coordinate system for the clinical description of three-dimensional motions: Application to the knee. *J. Biomech. Eng.* **1983**, *105*, 136–144. [CrossRef] [PubMed]
54. Minetti, A.E. A model equation for the prediction of mechanical internal work of terrestrial locomotion. *J. Biomech.* **1998**, *31*, 463–468. [CrossRef]
55. Blankevoort, L.; Huiskes, R.; de Lange, A. The envelope of passive knee joint motion. *J. Biomech.* **1988**, *21*, 705–720. [CrossRef]
56. Kadaba, M.P.; Ramakrishnan, H.K.; Wootten, M.E. Measurement of lower extremity kinematics during level walking. *J. Orthop. Res. Off. Publ. Orthop. Res. Soc.* **1990**, *8*, 383–392. [CrossRef]
57. Piazza, S.J.; Cavanagh, P.R. Measurement of the screw-home motion of the knee is sensitive to errors in axis alignment. *J. Biomech.* **2000**, *33*, 1029–1034. [CrossRef]
58. Cohen, J. *Statistical Power Analysis for the Behavioral Sciences*; Routledge: Abingdon-on-Thames, UK, 1988; ISBN 978-1-134-74270-7.
59. Zar, J.H. *Biostatistical Analysis*; Prentice Hall: Upper Saddle River, NJ, USA, 1999; ISBN 978-0-13-081542-2.

60. Folland, J.P.; Allen, S.J.; Black, M.I.; Handsaker, J.C.; Forrester, S.E. Running technique is an important component of running economy and performance. *Med. Sci. Sports Exerc.* **2017**, *49*, 1412–1423. [CrossRef]
61. Morin, J.B.; Samozino, P.; Zameziati, K.; Belli, A. Effects of altered stride frequency and contact time on leg-spring behavior in human running. *J. Biomech.* **2007**, *40*, 3341–3348. [CrossRef]
62. Altman, A.R.; Davis, I.S. A Kinematic Method for Footstrike Pattern Detection in Barefoot and Shod Runners. *Gait Posture* **2012**, *35*, 298–300. [CrossRef]
63. Larson, P.; Higgins, E.; Kaminski, J.; Decker, T.; Preble, J.; Lyons, D.; McIntyre, K.; Normile, A. Foot strike patterns of recreational and sub-elite runners in a long-distance road race. *J. Sports Sci.* **2011**, *29*, 1665–1673. [CrossRef]
64. Hasegawa, H.; Yamauchi, T.; Kraemer, W.J. Foot strike patterns of runners at the 15-km point during an elite-level half marathon. *J. Strength Cond. Res.* **2007**, *21*, 888–893. [CrossRef] [PubMed]
65. Kulmala, J.-P.; Avela, J.; Pasanen, K.; Parkkari, J. Forefoot strikers exhibit lower running-induced knee loading than rearfoot strikers. *Med. Sci. Sports Exerc.* **2013**, *45*, 2306–2313. [CrossRef] [PubMed]
66. Lyght, M.; Nockerts, M.; Kernozek, T.W.; Ragan, R. Effects of foot strike and step frequency on Achilles tendon stress during running. *J. Appl. Biomech.* **2016**, *32*, 365–372. [CrossRef]
67. Sinclair, J. Effects of barefoot and barefoot inspired footwear on knee and ankle loading during running. *Clin. Biomech.* **2014**, *29*, 395–399. [CrossRef] [PubMed]
68. Rooney, B.D.; Derrick, T.R. Joint contact loading in forefoot and rearfoot strike patterns during running. *J. Biomech.* **2013**, *46*, 2201–2206. [CrossRef] [PubMed]
69. Novacheck, T.F. The biomechanics of running. *Gait Posture* **1998**, *7*, 77–95. [CrossRef]